

Geophysical Research Letters®



RESEARCH LETTER

10.1029/2024GL110568

Unexpected STEVE Observations at High Latitude During Quiet Geomagnetic Conditions

Key Points:

- Non-storm and non-substorm Strong Thermal Emission Velocity Enhancement (STEVE) occurrence
- Strong subauroral flows during quiet geomagnetic conditions
- The ionospheric electrodynamics of this STEVE event differ from previous studies

Supporting Information:

Supporting Information may be found in the online version of this article.

Correspondence to:

B. Gallardo-Lacourt,
bea.gallardolacourt@nasa.gov

Citation:

Gallardo-Lacourt, B., Nishimura, Y., Kepko, L., Spanswick, E. L., Gillies, D. M., Knudsen, D. J., et al. (2024). Unexpected STEVE observations at high latitude during quiet geomagnetic conditions. *Geophysical Research Letters*, 51, e2024GL110568. <https://doi.org/10.1029/2024GL110568>

Received 18 JUN 2024







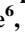


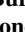

Accepted 18 SEP 2024

Author Contributions:

Conceptualization: B. Gallardo-Lacourt, Y. Nishimura, L. Kepko
Data curation: V. A. Pinto, D. Chaddock, J. Kuzub
Formal analysis: B. Gallardo-Lacourt, Y. Nishimura, J. K. Burchill, S. H. Skone, V. A. Pinto
Investigation: B. Gallardo-Lacourt, E. L. Spanswick, D. J. Knudsen, J. Kuzub, E. F. Donovan
Methodology: B. Gallardo-Lacourt, Y. Nishimura, L. Kepko, E. L. Spanswick, D. M. Gillies, D. J. Knudsen, J. K. Burchill, S. H. Skone, V. A. Pinto, J. Kuzub, E. F. Donovan
Software: B. Gallardo-Lacourt, E. L. Spanswick, D. M. Gillies, J. K. Burchill, S. H. Skone, V. A. Pinto

© 2024. The Author(s).

This is an open access article under the terms of the [Creative Commons Attribution-NonCommercial-NoDerivs License](https://creativecommons.org/licenses/by/4.0/), which permits use and distribution in any medium, provided the original work is properly cited, the use is non-commercial and no modifications or adaptations are made.

B. Gallardo-Lacourt^{1,2} , Y. Nishimura³ , L. Kepko¹ , E. L. Spanswick⁴ , D. M. Gillies⁵ , D. J. Knudsen⁴ , J. K. Burchill⁴ , S. H. Skone⁶, V. A. Pinto^{7,8} , D. Chaddock⁴ , J. Kuzub⁹ , and E. F. Donovan⁴ 

¹Goddard Space Flight Center, National Aeronautics and Space Administration, Greenbelt, MD, USA, ²Department of Physics, The Catholic University of America, Washington, DC, USA, ³Department of Electrical and Computer Engineering and Center for Space Physics, Boston University, Boston, MA, USA, ⁴Department of Physics and Astronomy, University of Calgary, Calgary, AB, Canada, ⁵Department of Chemistry and Physics, Mount Royal University, Calgary, AB, Canada, ⁶Department of Geomatics Engineering, University of Calgary, Calgary, AB, Canada, ⁷Departamento de Física, Universidad de Santiago de Chile, Santiago, Chile, ⁸Center for Interdisciplinary Research in Astrophysics and Space Sciences (CIRAS), Universidad de Santiago de Chile, Santiago, Chile, ⁹Citizen Scientist, Jufa Intermedia, Ottawa, ON, Canada

Abstract Strong Thermal Emission Velocity Enhancement (STEVE), is a captivating optical phenomenon typically observed in the mid-latitude ionosphere. This paper presents an intriguing observation of a STEVE event at high-latitudes, approximately 10 degrees poleward of previously documented observations. This event was recorded in Yellowknife, Canada, by a TREx RGB imager and a citizen scientist. Swarm satellites traversed the latitude of the observation, measuring extreme westwards ion drift velocities exceeding 4 km/s. Such velocities are more typically associated with the subauroral region located at mid-latitudes, rather than at the high-latitudes reported here. Significantly, this event occurred without a substorm, which differs from previous STEVE observations. While high-latitude radars detected fast ionospheric equatorward flows, GOES satellite did not record any injections. These observations suggest that the inner magnetosphere is highly inflated. This unique case study raises new questions surrounding subauroral dynamics and the influence of magnetospheric configurations on ionospheric responses.

Plain Language Summary Strong Thermal Emission Velocity Enhancement, also known as STEVE, is a fascinating nighttime optical phenomenon that takes place in the upper part of Earth's atmosphere. It can be easily recognized by its distinctive appearance as a narrow white-mauve arc that is associated with strong westward flows and is situated just equatorward of the auroral oval. Previous research has shown that STEVE events occur together with intense ionospheric flows and occur after specific disturbances in the near-Earth space environment known as substorms. They have found that substorms are important for creating the special conditions that lead to STEVE and other subauroral enhancements. In our study, we focus on a unique STEVE event that did not occur after a substorm. Furthermore, this observation took place under remarkably quiet solar wind conditions; nevertheless, strong ionospheric flows were recorded. This unusual case raises new questions about the atmospheric responses and how it is affected by the configuration of the magnetic field in space. By investigating these special circumstances, we hope to learn more about STEVE and its causes, which will help us advance our knowledge in the complex ionosphere-magnetosphere-solar wind coupled system.

1. Introduction

The subauroral ionosphere, situated immediately equatorward from the auroral oval, exhibits a diverse array of dynamic processes (e.g., Gallardo-Lacourt et al., 2021; E. Mishin & Streltsov, 2021). The subauroral region lies around the nightside transition region, where the magnetic field configuration shifts from stretched field lines in the plasmasheet to a more dipolar configuration of the inner magnetosphere. Hence, the subauroral region is influenced by the plasma sheet, the ring current, the plasmasphere, and the thermosphere-ionosphere system. Among the well-known phenomena in this region are Subauroral Polarization Streams or SAPS, characterized by westward flow enhancements within a region of reduced plasma density known as the plasma trough (Foster & Burke, 2002).

The term SAPS encompasses two phenomena in the subauroral ionosphere: latitudinally wide flows ($\sim 5^\circ$ latitude) with westward-directed velocities of approximately 500 m/s, and narrow ($\sim 1^\circ$ latitude) and rapid (>1 km/s)

Supervision: L. Kepko

Visualization: B. Gallardo-Lacourt,
V. A. Pinto, D. Chaddock, J. Kuzub

Writing – original draft: B. Gallardo-Lacourt

Writing – review & editing: B. Gallardo-Lacourt, Y. Nishimura, L. Kepko,
D. M. Gillies, D. J. Knudsen, J. K. Burchill,
S. H. Skone, V. A. Pinto, D. Chaddock,
J. Kuzub

westward plasma flows, recognized as polarization jets or subauroral ion drifts (SAIDs). In addition to SAIDs, a second category, primarily observed during quiet geomagnetic conditions, has been termed Birkeland Current Boundary Flows (BCBF) (Archer et al., 2017). While SAIDs and BCBFs share similar westward flow magnitudes, they differ in their location relative to field-aligned currents (FACs), temperature magnitude, and the clear morphology of a plasma trough (Archer & Knudsen, 2018).

SAIDs are most often observed during the recovery phase of a substorm and have been well-observed by satellites and ground-based instruments (Anderson et al., 1991, 1993, 2001; Foster et al., 1994; Galperin, 2002; He et al., 2014; Maynard et al., 1980; E. V. Mishin, 2023; Nishimura et al., 2022). A statistical study using a large number of events (over 15,000) detected by DMSP satellites showed that most SAIDs occur at about $60^\circ \pm 5^\circ$ of magnetic latitude at around 22 magnetic local time (MLT) (He et al., 2014). This location is typically considered as the poleward section of the mid-latitude ionosphere (Heelis, 2004; Laakso & Pfaff, 2023).

In recent years, collaborative investigations between professional scientists and citizen scientists have helped us identify an optical signature related to SAIDs (Gallardo-Lacourt et al., 2019; MacDonald et al., 2018; Nishimura et al., 2023). This phenomenon, known as Strong Thermal Emission Velocity Enhancement (STEVE), can be observed in the night sky as a latitudinally narrow ($<1^\circ$, or about 100 km) mauve arc spanning several hours in MLT and located equatorward of the auroral oval. STEVE is closely associated with strong SAIDs which are characterized by velocities exceeding 3 km/s, very high electron temperatures, and narrow downward region-2 FACs just equatorward of the sharp electron precipitation boundary (Archer et al., 2019; MacDonald et al., 2018; Nishimura et al., 2023).

Previous studies of STEVE have revealed several distinctive characteristics. Utilizing POES satellite data, a case study demonstrated that STEVE is not connected to particle precipitation, thus distinguishing it from traditional auroras (Gallardo-Lacourt, Liang, et al., 2018). This initial finding was further supported by an analysis of conjugated observations of STEVE events, combining ground-based instruments and multi-satellite observations, which suggested that STEVE is driven by heating mechanisms within the ionosphere (Nishimura et al., 2019). Additionally, measurements of the STEVE spectrum using the recently deployed Transition Region Explorer (TReX) spectrograph of the University of Calgary have demonstrated that STEVE exhibits a continuous spectrum (Gillies et al., 2019), which indicates collisional heating rather than particle precipitation.

A statistical study by Gallardo-Lacourt, Nishimura, et al. (2018) shed further light on STEVE's optical characteristics and the geomagnetic conditions under which STEVE is typically observed. The study revealed that, on average, the duration of STEVE events is approximately 1 hour. It is noteworthy that all the STEVE events reported in this study were located within the magnetic latitudes of $59\text{--}63^\circ$, consistent with the statistical location of SAIDs reported by He et al. (2014). In addition, Gallardo-Lacourt, Nishimura, et al. (2018) found that, statistically, STEVE occurs during relatively moderate geomagnetic conditions measured by D_{st} decreases of around 30 nT, toward the end of an extended substorm expansion phase, and is associated with $K_p \sim 4$. These findings suggest the potential involvement of the magnetosphere in supplying energy and creating specific ionospheric conditions that give rise to STEVE. However, it is not understood why STEVE occurrences tend to favor moderate geomagnetic conditions, while STEVE itself remains rare. Despite the frequent occurrence of moderate conditions, only about 40 events have been analyzed in the literature.

More recently, Svaldi et al. (2023) conducted a comprehensive analysis of high latitude ionospheric dynamics using the state-of-the-art Assimilative Mapping of Geospace Observations (AMGeO, AMGeO Collaboration, 2019) for over 30 observed STEVE events and regular non-STEVE substorms with similar magnitudes to those preceding the STEVE observations. This investigation highlighted that the substorms observed prior to STEVE events resulted in larger enhancements of cross-polar cap potential drops compared to the non-STEVE substorms. Additionally, the high latitude convection pattern obtained through AMGeO revealed a pronounced and prolonged Harang reversal, which could potentially contribute to the intensification of subauroral electric fields responsible for the significant SAIDs observed for STEVE in earlier studies. Furthermore, the AMGeO results show that the dawn cell extends further into the pre-midnight sector, likely correlating with the large westward motion of the surge and streamers that contribute to injections at the local time of STEVE occurrence, in line with previous research findings (Nishimura et al., 2020).

In summary, STEVE typically emerges at the end of an extended substorm expansion phase, during moderate geomagnetic conditions. It is commonly associated with extreme SAIDs, statistically observed around 60°

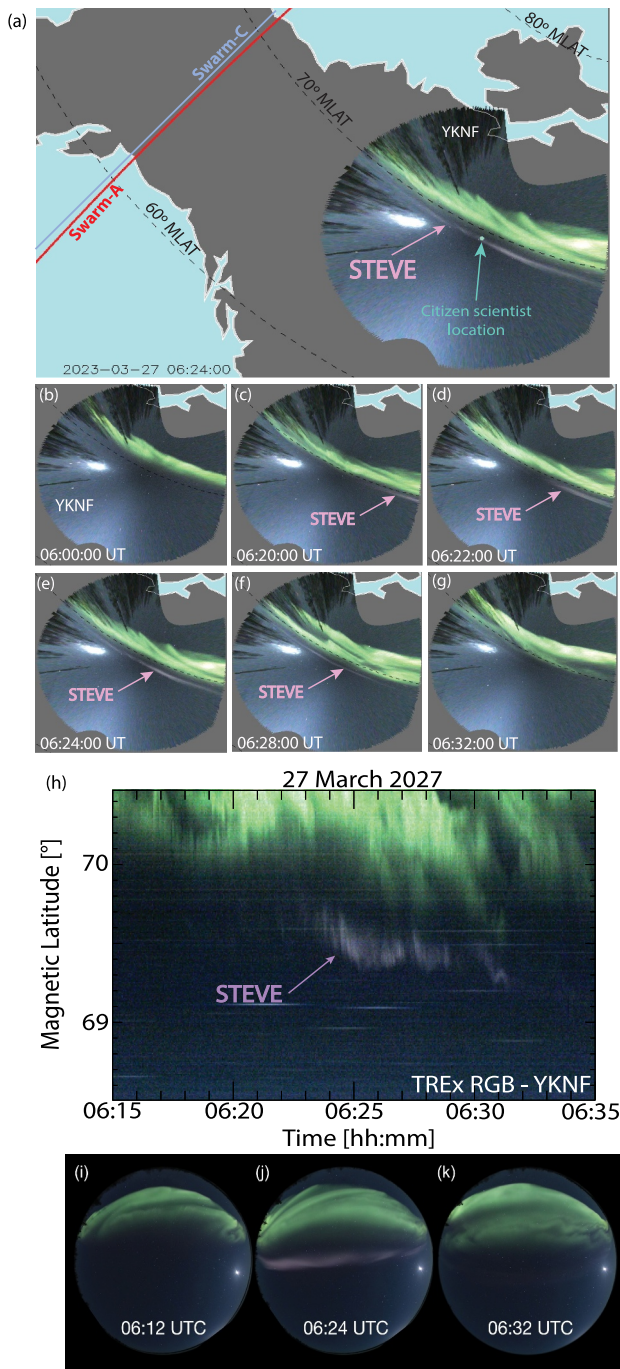


Figure 1. STEVE observations on 27 March 2023. (a) Map indicating the location of the TReX RGB imager at Yellowknife (YKNF), the citizen scientist (green), and Swarm satellite (A in red and C in light blue) (b–g) Sequence with the evolution of the STEVE observation made by the TReX RGB imager at YKNF operating in burst mode (3 Hz). (h) Keogram from the TReX-RGB at YKNF summarizing the observation. (i–k) Citizen scientist's observation captured with one of the AurorEye imaging systems developed and operated by citizen scientists.

magnetic latitude. However, in this paper, we present a STEVE event occurring at approximately 69° magnetic latitude, where no evident substorm was observed. These observations challenge our current understanding of STEVE and prompt new inquiries into the generation mechanisms of SAIDs and the impact of diverse magnetospheric configurations.

2. Data Sets and Methodology

The STEVE event described in this paper was observed on 27 March 2023, at Yellowknife (YKNF), Canada, in the Northwestern Territories. The event was captured by one of the RGB all-sky imagers (ASIs) from the Transition Region Explorer (TReX) array, deployed and operated by the University of Calgary. The TReX array consists of seven true color or RGB imagers that cover a large section of Canada. Additionally, the array includes blue-line and near-infrared ASIs, riometer, and spectrographs (Liang et al., 2024). Although the nominal temporal resolution of the TReX-RGB array is 3 s, the YKNF RGB imager that captured the STEVE event was operating in a 3 Hz burst mode. Figure 1a illustrates the instruments used in this study and their respective locations.

In addition to the TReX RGB observation, a citizen scientist positioned slightly east of the center of the YKNF TReX RGB also captured the formation of STEVE (see Figure 1a). Citizen science has played a crucial role in understanding the dynamics and characteristics of STEVE (e.g., Nishimura et al., 2023). Citizen science initiatives connect scientists with the public, enabling discovery and engaging broad audiences worldwide (Ledvina et al., 2023). These individuals possess the skills and enthusiasm to capture observations of scientific phenomena, such as STEVE. The observation reported in this paper was captured by Jeremy Kuzub, a citizen scientist who developed a project called AurorEye. AurorEye is a highly portable, autonomous, self-contained, full-color all-sky imaging system optimized for quick field setup to capture time-lapse aurora photography. The design, construction, testing, deployment, and operation of AurorEye units are carried out by citizen scientists.

Furthermore, two of the European Space Agency's Swarm satellites were in the vicinity of the TReX RGB location. The Swarm satellites measure electric and magnetic fields, in addition to electron density and temperature, within the altitude range of 400–500 km (Knudsen et al., 2017; Merayo et al., 2008). The data regarding plasma density and electron temperature are sourced from the Langmuir probe (LP) extended data set. Ion velocity (V_i) in this study is derived from the 16-Hz thermal ion imager cross-track data set. In addition, the FAC measurements presented here are obtained from a single-satellite magnetometer and assume that the satellites are crossing a static and infinite current sheet at normal incidence.

Swarm-A and C crossed the subauroral region approximately 15 min earlier (between 06:03:30–06:04:00 UT) than the STEVE observations and was positioned three hours westward in MLT compared to the TReX STEVE observation. Figure 1a shows the orbit of Swarm-A in red and Swarm-C in green. Although the TReX-RGB at YKNF was not exactly collocated with the Swarm satellite trajectory, the zonal alignment of both SAIDs and STEVE allows for a meaningful comparison. A similar approach of using near-coincident measurements was used by Archer et al. (2019) when analyzing the SAID characteristics of STEVE events.

Solar wind conditions are from the OMNI database, while the SML index was obtained from the SuperMAG data set (Gjerloev, 2012). We utilize the 1-min OMNI data set (King & Papitashvili, 2005), which includes bow shock nose-shifted solar wind magnetic field and plasma data from Wind and ACE satellites. SuperMAG indices are derived from ground magnetometer stations situated between 40°N and 80°N. A comprehensive explanation of the index derivation has been described by Newell and Gjerloev (2014).

We utilized data from the GOES-18 satellite to investigate the presence of injections at geosynchronous orbit. GOES-18 is a part of the GOES-R series, equipped with a suite of instruments designed to detect and monitor approaching space weather hazards. Specifically, we employed the Space Environment In Situ Suite (SEISS) instrument to measure plasma properties and energetic particle populations. Our analysis focused on the 1-min average differential fluxes from the Magnetospheric Particle Sensors (MPS-HI and MPS-LO).

We estimated the location of the plasma trough and plasmasphere by identifying the maximum electron density in the F2 layer, using a model that employs a unique data assimilation approach tailored for high latitudes. For this STEVE event, total electron content (TEC) data were assimilated from 150 GNSS stations spanning mid-latitudes to the polar region in the Northern Hemisphere. This method enables us to accurately resolve both the vertical and horizontal electron density distribution across the entire area (Skone & Spanswick, 2023).

Finally, we utilize SuperDARN flow vector data to analyze fast flows within the polar cap, the auroral oval, and the subauroral regions. Flow vectors are derived from all available data obtained from the Super Dual Auroral Radar Network (SuperDARN) line-of-sight (LOS) measurements. Utilizing the divergence-free condition (Bristow et al., 2016, 2022), we employ the Spherical Elementary Current Systems (SECS) technique (Amm et al., 2010) to obtain a 2-day divergence-free flow pattern from the LOS SuperDARN velocities. This method yields a divergence-free solution at 0.5° latitude and 1.5° longitude grids where echoes exist and at a 1° latitude and 3° longitude grid elsewhere. It excludes a background statistical convection model to prevent the influence of prescribed background flows, thus emphasizing the continuity of observed flow channels, which are best represented by the line-of-sight (LOS) data (Lyons et al., 2024; Nishimura et al., 2023, 2024). In this paper, we utilize SuperDARN flow vector data to analyze fast flows within the polar cap, the auroral oval, and the subauroral regions.

3. Event Description: 27 March 2023

During the event on 27 March 2023, the auroral oval, which is confined very poleward but visible in the northern region (toward the top) of the YKNF ASI (Figure 1b), appears active. At about 06:18:00UT an initially faint STEVE appeared in the eastward portion of the ASI and rapidly propagated across the camera field-of-view (FOV) (Figures 1c–1e). STEVE starts becoming fainter at about 06:28:00UT (Figure 1f) and by 06:32:00UT (Figure 1g) the structure is no longer visible. Figure 1h shows a keogram of the YKNF ASI where STEVE is clearly observed located equatorward of the poleward boundary of the auroral oval. It is important to highlight that during this time, all the other available cameras from TREx, THEMIS, and REGO (Red-line Emission Geospace Observatory) ASIs did not show any auroral structure southward of the STEVE observation. Additionally, DMSP satellite measurements in the pre-midnight sector indicate that, at the time of the STEVE observation, the equatorward boundary of the auroral oval extended above 70° magnetic latitude. Figure S1 in the Supporting Information S1 presents overview plots from the DMSP-17 and DMSP-18 satellites, located in the Southern Hemisphere, illustrating these observations.

Besides the STEVE observation by TREx, Figures 1i–1k show the citizen scientist's observation of STEVE. This observation was captured by the AurorEye Citizen Science Project which is a highly portable, autonomous, self-contained, full-color all-sky imaging system optimized for quick field setup to capture all-sky time-lapse aurora photography. Similarly to the TREx observation, the citizen scientist data shows the mauve structure known as STEVE very clearly across the center of the camera FOV. For videos of this observation captured by the TREx-RGB at YKNF and the AurorEye citizen scientist project, please refer to Supporting Information Movies M1 and Movie M2 respectively.

In addition to the optical data, the Swarm-A satellite crossed the subauroral region approximately 3 hr in MLT west of the YKNF observation (19 MLT vs. 22 MLT) and about 10 min earlier (Figure 2). Swarm observations indicated that the subauroral region was located at ~70° magnetic latitude (MLAT) and detected fast westward flows exceeding 4 km/s (Figure 2a). These flows were primarily located in the Region 1 (R1) portion of the field-

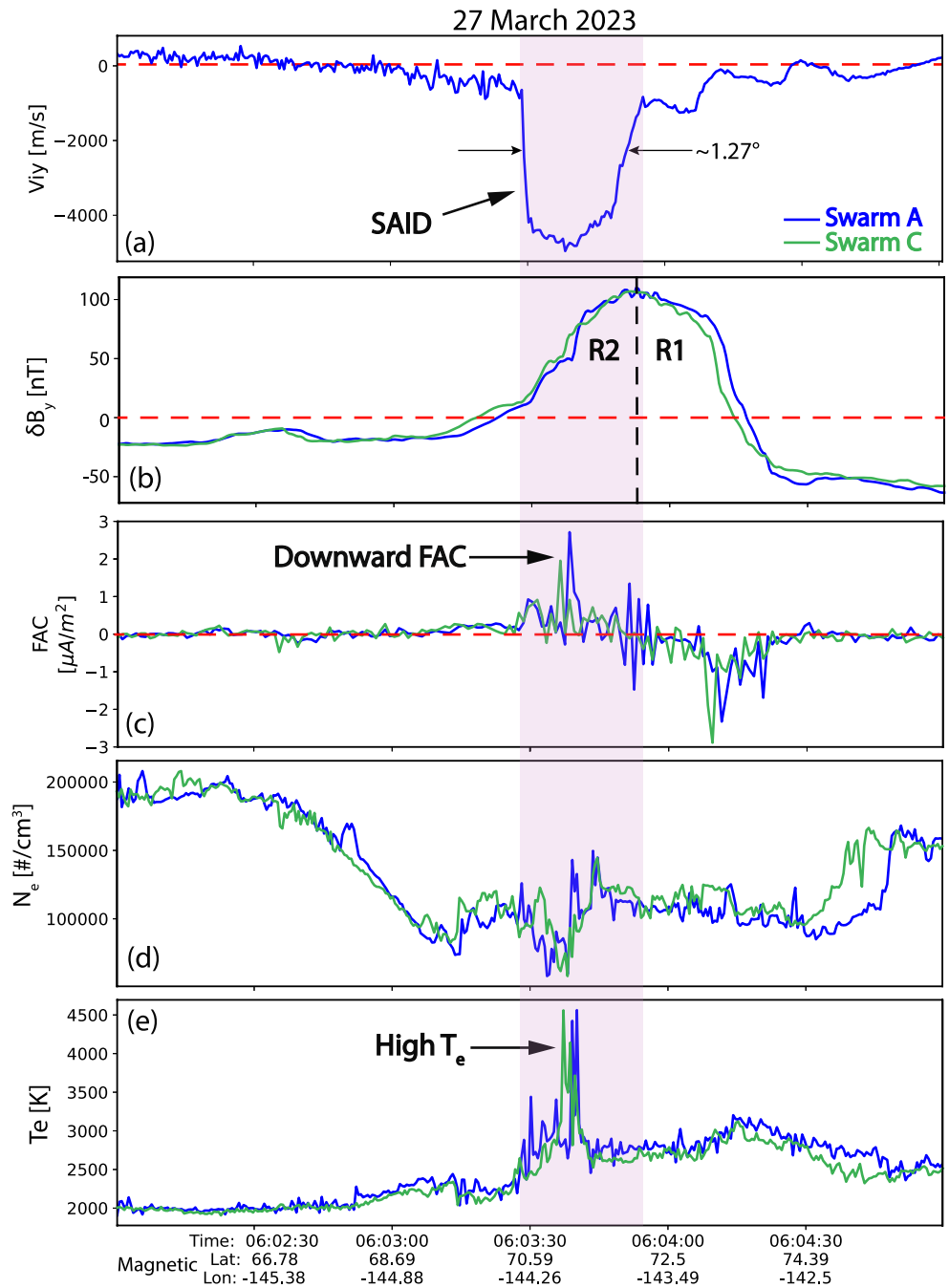


Figure 2. Swarm satellite data during the STEVE event observed on 27 March 2023. From top to bottom, the panels represent (a) ion flow velocity (V_i) in m/s, (b) magnetic field perturbations in the y-component (δB_y) to infer R1 and R2 FACs, (c) vertical component of field-aligned currents (FAC) in $\mu\text{A}/\text{m}^2$, (d) electron density (N_e) in cm^{-3} , and (e) electron temperature (T_e) in Kelvin. Swarm-A is shown in blue, and Swarm-C is shown in green. The purple area indicates the subauroral measurements taken around the same latitude as the STEVE observation.

aligned currents (FACs) (Figure 2b), characterized by downward FACs (as indicated by the vertical component of current density in Figure 2c), low electron density (Figure 2d), and very high electron temperatures reaching approximately 4,500 K (Figure 2e). The Swarm measurements are consistent with those previously observed during typical STEVE occurrences (e.g., Archer et al., 2019; MacDonald et al., 2018), but they are approximately 10° northward from where the subauroral region is typically observed (e.g., He et al., 2014; Nishimura

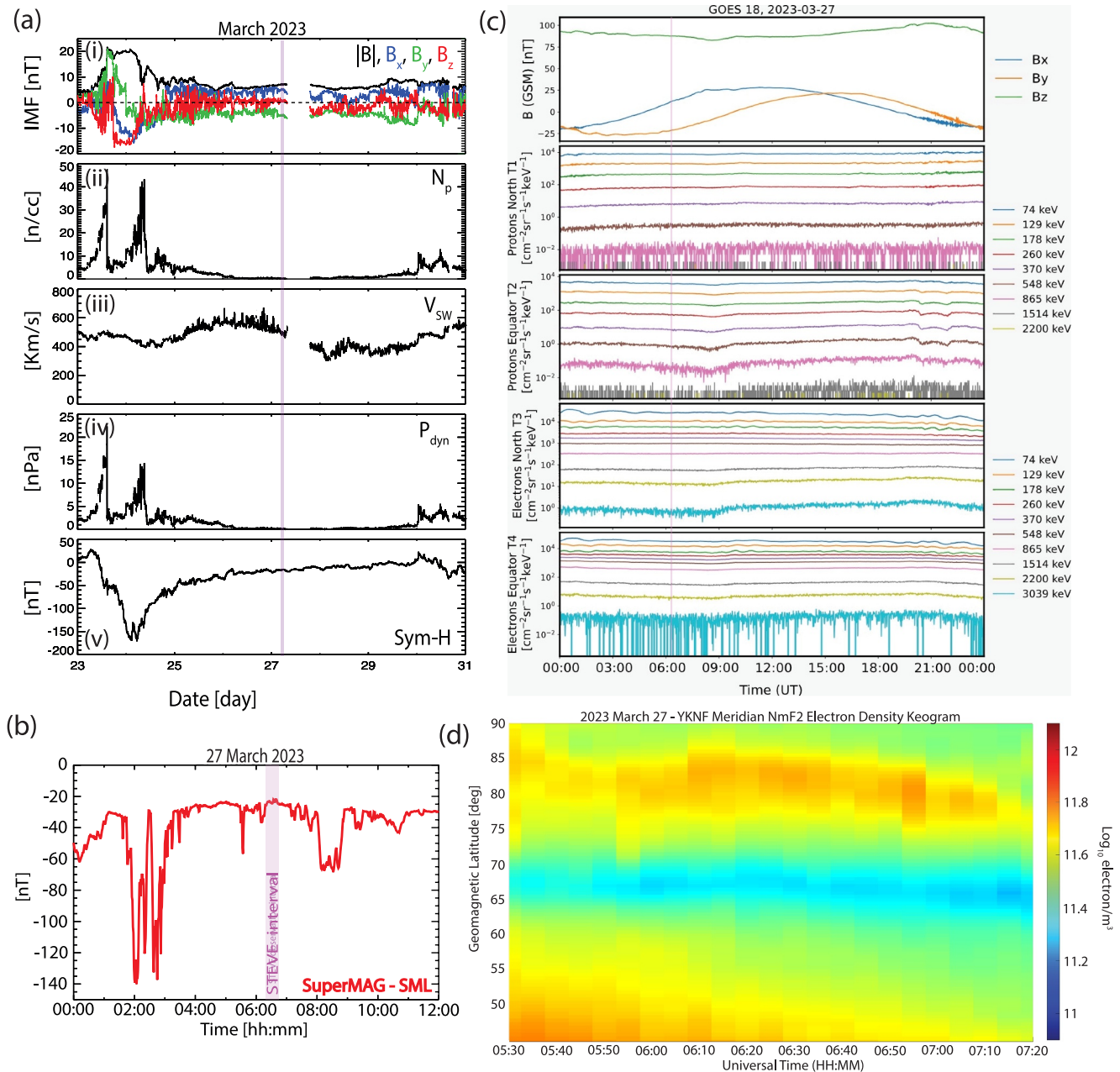


Figure 3. (a) Solar wind conditions obtained from the OMNI database. From top to bottom, the panels represent (i) interplanetary magnetic field (IMF), (ii) solar wind density, (iii) solar wind speed, (iv) solar wind pressure, and (v) Sym-H index. (b) SML index obtained from the SuperMAG database. (c) GOES-18 satellite measurements at geosynchronous orbit. (d) Peak electron density values along the Yellowknife (geomagnetic) meridian. These values occur typically near 350 km altitude. Lower values correspond to plasma trough location.

et al., 2022). In addition, Swarm-C (shown in green in Figure 2) was slightly less than 70 km behind Swarm-A, with an east-west separation of about 40 km. Panel a in Figure 2 shows the cross-track ion drift from Swarm-A only, where positive values represent approximately eastward drifts. There was insufficient ion signal in the Swarm C Thermal Ion Imagers to provide reliable estimates of ion drift. However, it is important to note that all the other parameters measured by Swarm-C are consistent with those observed by Swarm-A. The overall pattern of FAC is similar, and both satellites measured a large downward FAC at the center of the SAID.

Figure 3a shows the solar wind conditions for this event. A geomagnetic storm started on 23 March 2023, and reached a SYM-H minimum value of ~ -150 nT on March 24 (Figure 3a Panel v). STEVE occurred toward the

end of the recovery phase of the storm when SYM-H was approximately -15 nT. The vertical purple line in Figure 3a corresponds to the time when STEVE was observed. During the time of the STEVE event, the Interplanetary Magnetic Field (IMF) B_y component was predominantly negative, with the B_z component exhibiting northward orientation during the event. These conditions persisted for several hours leading up to the event (Figure 3a). Additionally, the very low solar wind density ranging between 0.2 and 0.3 [1/cc] (Figure 3a Panel ii) and the solar wind velocity (Figure 3a Panel iii) was approximately 500 km/s. Importantly, the solar wind Mach number (not shown) remains low, fluctuating around 3 the day prior to the event and decreasing to approximately 1.5 several hours before the STEVE observation. During this period, the magnetosphere undergoes significant expansion, contributing to the conditions leading up to the STEVE event. The SuperMAG SML index (Figure 3b) was relatively quiet at about -30 nT. While a decrease in SML of about -140 nT was observed several hours earlier, SML was quiet and never reached below -60 nT for at least three hours prior to the observation of STEVE. Furthermore, in line with these quiet conditions, SuperDARN convection patterns aligned with non-substorm events observed during negative IMF B_y conditions (see Figure S1 in the Supporting Information S1), as detailed by Grocott et al. (2010). Given the solar wind conditions, it is unsurprising that these convection patterns differ significantly from those reconstructed by Svaldi et al. (2023) for over 30 STEVE observations.

GOES-18 mapped to a position equatorward of the observation area. Figure 3c shows GOES-18 SEISS 1-min averaged differential fluxes from the Magnetospheric Particle Sensors (Kress et al., 2020). The satellite did not detect any injections at geosynchronous orbit in either of the two telescopes for protons (second and third panel) or electrons (fourth and fifth panel).

The electron density as functions of latitude and time from YKNF are presented in Figure 3d. The plasma trough is indicated by low densities (blue), while the plasmasphere and the auroral oval are characterized by higher densities shown in warmer colors (red and yellow). Note that the plasma trough becomes more depleted approximately 20 min before the STEVE event. Interestingly, the modeled plasma trough is located at least 5° poleward of the statistical locations calculated from similar events (Pedatella & Larson, 2010; Starr et al., 2022). The high latitude location of the auroral oval, combined with the measurements of the GOES satellite and the electron density distributions, potentially suggests that the plasmasphere has expanded beyond geosynchronous orbit in the tailward direction.

Figure 4 presents the SuperDARN flow vectors, utilizing data from the entire network. The diagram features colored arrows to denote the SuperDARN flows, with a red vertical line marking magnetic noon and a blue one for magnetic midnight. The STEVE phenomenon was recorded approximately 2 hours before midnight MLT, at the YKNF location, which is highlighted in red. In Figure 4, panel a demonstrates by the colored arrows that rapid flows are confined mostly at higher latitudes, likely within both the polar cap and auroral oval. At 06:10 UT, the vicinity of YKNF shows weak flows, approaching 0 m/s. However, from 6:12 to 6:18 UT, as illustrated in panels b to d of Figure 4, there is a noticeable intensification of fast flows from higher latitudes, with a distinct flow channel, highlighted by a black arrow, extending from very high latitudes down to $\sim 75^\circ$ magnetic latitude. Concurrently, flows near YKNF also increased, reaching speeds close to 800 m/s. This intensification persisted even after the high latitude flows diminished, as shown in panel e. The flow direction is westward, aligning with typical subauroral flow patterns. By 6:36 UT, as depicted in panel f, there is a marked reduction in flows both at high latitudes and in the subauroral region, coinciding with the disappearance of STEVE from the YKNF field of view.

4. Discussion and Conclusion

In this study, we report on a STEVE observation made during the late recovery phase of a geomagnetic storm. The auroral oval was positioned at very high latitudes ($>70^\circ$ mlat), as evidenced by the absence of aurora southward of the STEVE observation and DMSP satellite measurements indicating the equatorward boundary of the auroral oval was located above 70° magnetic latitude (see Figure S2 in the Supporting Information S1). Importantly, a recent re-analysis of Dynamics Explorer-2 satellite data (Laakso & Pfaff, 2023) has revealed the occurrence of fast plasma drifts at high latitudes. The observation presented here supports that study's suggestion that some of the fast plasma drifts observed at high latitudes could correspond to subauroral ion drifts.

In addition to the unusually high latitude location of this STEVE observation, the geomagnetic conditions during this event differ from those typically associated with STEVE or SAIDs in general. As stated in the introduction,

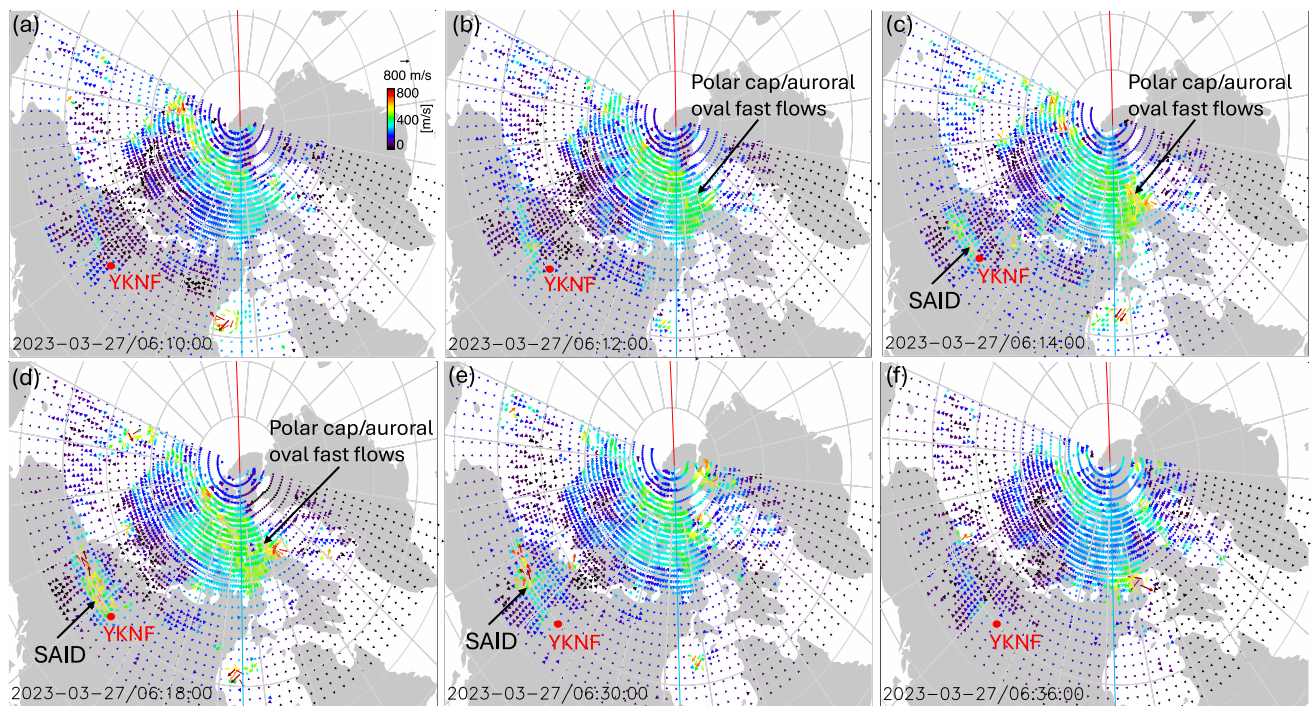


Figure 4. Flow vectors are derived from SuperDARN LOS measurements. The arrows indicate the direction of the flow and the color corresponds to the magnitude. Vertical blue and red lines correspond to magnetic noon and midnight respectively. The location of the YKNF TREX ASI is marked in red.

typical SAID and STEVE observations manifest under moderate to active geomagnetic conditions (e.g., Anderson et al., 1991; Anderson et al., 1993; Gallardo-Lacourt et al., 2021; Gallardo-Lacourt, Nishimura, et al., 2018; Galperin, 2002; Martinis et al., 2022), typically marked by the presence of auroral substorms preceding these observations. In general, auroral substorms are characterized by the poleward and equatorward expansion of the auroral oval (Akasofu, 1964). Apart from the optical characteristics, substorms are usually identified by variations in geomagnetic indices such as AL or SML (e.g., Newell & Gjerloev, 2011). An intriguing aspect of the event presented here is that it unfolds under geomagnetic conditions conventionally considered quiet. Interestingly, despite the activity at high latitudes, the auroral oval does not expand equatorward at any point before or during the event, which suggests that this event does not follow the pattern observed in typical STEVE events, which usually occur after a substorm (see Figures 1b–1g and Movie M1 in the Supporting information).

While the Dst index for STEVE events was analyzed in a statistical study by Gallardo-Lacourt, Nishimura, et al. (2018), the ± 12 -hr time window selected to visualize the variations of the index was not adequate to assess storm-time conditions. Upon re-analyzing all available 32 STEVE events utilized in the Svaldi et al. (2023) study, it was observed that there is a clear reduction of the Dst index reaching close to -30 nT (See Figure S3 in the Supporting Information S1), which has been categorized as a small geomagnetic storm in the literature (e.g., Gonzalez et al., 1994; Yokoyama & Kamide, 1997). Considering this together with previously reported storm-time STEVE event (e.g., Martinis et al., 2022), we can conclude that unlike the event reported here, typical STEVE events are storm-time phenomena occurring during the main phase of the storm.

The conditions observed during this event bear similarity to those documented on 11 May 1999, known as *The Day the Solar Wind Disappeared* (e.g., Le et al., 2000). Simulation results of ring current dynamics during this event suggested that traditional geomagnetic indices like Dst or Sym-H may not reliably reflect the lower limit of ring current activity (Jordanova et al., 2001). This implies that although Sym-H remains relatively stable around -16 nT before and during the STEVE event, the ring current may still be active, potentially influencing the dynamics of the subauroral region.

In addition, analysis of GOES satellite data reveals the absence of particle injections at geosynchronous orbit. Considering the presence of a fast flow channel detected by SuperDARN and the positioning of the auroral oval at

high latitudes, this potentially suggests an extension of the plasmasphere beyond geosynchronous orbit. This is supported by the electron density that shows that the plasmasphere has expanded to high latitudes reaching about 69° magnetic latitude. While this aspect will be further investigated in subsequent research, previous studies in the literature (e.g., Grocott et al., 2010) have examined the influence of IMF B_y on the evolution of ionospheric convection, concluding that when IMF is northward with a significant B_y component, as is the case in the event presented here (where IMF B_z is positive for at least 2 hours prior, during, and after the event, and B_y has a magnitude of about 5 nT), low-latitude reconnection is maintained at a rate sufficient to gradually inflate the magnetotail but insufficient to drive the substorm cycle (e.g., Grocott et al., 2003; Milan et al., 2005; Sandholt et al., 1998). Moreover, these studies have reported a lack of associated substorm signatures, such as geosynchronous particle injections and global auroral expansions, implying that reconnection could be occurring at a more distant neutral line, rather than the near-Earth neutral line activated at substorm onset.

While previous studies of ionospheric plasma convection offer insights into magnetospheric configuration during such events, magnetospheric modeling under the conditions reported here could provide a deeper understanding of magnetotail dynamics and evolution. Additionally, these ionospheric studies do not shed light on the drivers of these strong SAIDs. From an ionospheric perspective, it is widely accepted that the strong, localized ionospheric flows of SAIDs are associated with strong conductivity gradients in the region (Figueiredo et al., 2004; Lin et al., 2021; Lynch et al., 2022; Zettergren & Snively, 2019). However, they do not elucidate the role of substorms and substorm injections, which have been widely discussed in the literature as potential mechanisms for SAID generation, such as the current and voltage generators paradigms, among others (Anderson et al., 1991; Anderson et al., 1993; E. V. Mishin & Puhl-Quinn, 2007; E. V. Mishin, 2013).

Lastly, the variations in the FAC measured by Swarm-A and Swarm-C between 06:03:40 UT and 06:04:10 UT are well above noise levels, suggesting the presence of either filamentary currents or Alfvén wave activity. It is also worth noting that the width of the SAID, 1.27° (approximately 150 km), is much larger than the apparent width of STEVE (see Figure 1h). Notably, the observation of fast flows during quiet conditions between R1 and R2 suggests that this event could be consistent with BCBFs (Archer & Knudsen, 2018), which aligns with proposed generation mechanisms that only require a threshold on the flow speed (Harding et al., 2020). However, the clear identification of a trough, combined with the extreme electron temperatures measured by Swarm and the DMSP particle precipitation data indicating that these fast flows are located in the subauroral ionosphere, suggests that the event reported here is more likely associated with SAID. Nonetheless, further analysis of the relationship between continuum emissions and fast ionospheric flows, such as BCBFs, could enhance our understanding of newly reported phenomena, including post-midnight purple arcs (Nanjo et al., 2024). Interestingly, Swarm satellite data from the subsequent orbit, following the STEVE event reported in this paper, reveals a fast SAID measurement. Simultaneously, both the AurorEye and TREx RGB systems detected a thin, continuum emission (see Figure S4 in the Supporting Information S1).

This paper raises new questions not only about STEVE generation mechanisms but also about the processes behind the generation of subauroral electric fields, one of the most fascinating and debated phenomena in the ionosphere-magnetosphere coupled system. Further analysis and future missions, such as the next NASA Geospace Dynamics Constellation, should help unravel the mechanisms driving the diverse dynamics in the subauroral region.

Data Availability Statement

The Transition Region Explorer RGB (TREx RGB) is a joint Canada Foundation for Innovation and Canadian Space Agency project developed by the University of Calgary. TREx RGB is operated and maintained by Space Environment Canada with the support of the Canadian Space Agency (CSA) [23SUGOSEC] (Spanwick & Donovan, n.d.). The TREx RGB data can be obtained from https://data.phys.ucalgary.ca/sort_by_project/TREx/RGB/stream0/2023/03/27/yknf_rgb-08/ut06/. The Swarm data are provided by the European Space Agency with additional processing supported by Canadian Space Agency Grant 15SUSWARM. The Swarm data is available at <https://earth.esa.int/eogateway/missions/swarm/data> data access. We also acknowledge the use of the SuperMAG index SML indices (Newell & Gjerloev, 2011) which can be downloaded from <https://supermag.jhuapl.edu/indices/>. The OMNI data were obtained from the GSFC/SPDF OMNIWeb interface and can be acquired at <https://omniweb.gsfc.nasa.gov>. GOES-18 satellite data can be obtained from <https://data.ngdc.noaa.gov/platforms/>

solar-space-observing-satellites/goes/goes18/12/data/mpsh-l2-avg1m/2023/03/. SuperDARN data can be downloaded from <https://superdarn.jhuapl.edu/download>. The overview plots of SuperDARN convection maps can be viewed at <https://superdarn.ca/convection-maps>. DMSP data can be obtained here <https://cdaweb.gsfc.nasa.gov/>. To download the SuperDARN and DMSP data, readers need to select the event date (2023-03-27) and click "Download" to generate the files. Citizen scientist's data from the AurorEye Project can be visualized via the link <https://auroreye.ca/> and obtained by request to Jeremy Kuzub.

Acknowledgments

BGL and LK are supported by the NASA Mesoscale Magnetospheric Dynamics Heliophysics Internal Science Funding Model (HISFM). The work of YN was supported by NASA Grants 80NSSC20K0725, 80NSSC21K1321, 80NSSC22K0323, 80NSSC22K0749, 80NSSC23M0193 and 80NSSC23K0410, NSF Grants AGS-1907698 and AGS-2100975, and AFOSR Grants FA9559-16-1-0364 and FA9550-23-1-0614. VP thanks ANID SIA Grant SA77210112 and DICYT Regular Grant 042431PA. JKB was supported from Canadian Space Agency Grant 15SUSWARM. BGL wants to thank Robert Robinson, Doug Rowland, Mark Adrian, and Shing Fung for very useful discussions. The authors thank Dr. W. E. Archer for his careful review that has significantly improved this paper. The authors also thank the STEVE Workshop supported by NSF (AGS-2025481) for useful discussions during and after the meeting with the participants. This research was supported by the International Space Science Institute (ISSI) in Bern and Beijing, through ISSI International Team projects Auroral Research Coordination: Towards Internationalized Citizen Science (ARCTICS), Multi-Scale Magnetosphere-Ionosphere-Thermosphere Interaction, and Magnetotail Dipolarizations: Archimedes Force or Ideal Collapse?.

References

- Akasofu, S.-I. (1964). The development of the auroral substorm. *Planetary and Space Science*, 12(4), 273–282. [https://doi.org/10.1016/0032-0633\(64\)90151-5](https://doi.org/10.1016/0032-0633(64)90151-5)
- AMGeO Collaboration. (2019). *A collaborative data science platform for the geospace community: Assimilative mapping of geospace observations (AMGeO) v1.0.0 (Tech. Rep.)*. Zenodo. <https://doi.org/10.5281/zenodo.3564914>
- Amm, O., Grocott, A., Lester, M., & Yeoman, T. K. (2010). Local determination of ionospheric plasma convection from coherent scatter radar data using the secs technique. *Journal of Geophysical Research*, 115(A3). <https://doi.org/10.1029/2009JA014832>
- Anderson, P. C., Carpenter, D. L., Tsuruda, K., Mukai, T., & Rich, F. J. (2001). Multisatellite observations of rapid subauroral ion drifts (said). *Journal of Geophysical Research*, 106(A12), 29585–29599. <https://doi.org/10.1029/2001JA000128>
- Anderson, P. C., Hanson, W. B., Heelis, R. A., Craven, J. D., Baker, D. N., & Frank, L. A. (1993). A proposed production model of rapid subauroral ion drifts and their relationship to substorm evolution. *Journal of Geophysical Research*, 98(A4), 6069–6078. <https://doi.org/10.1029/92JA01975>
- Anderson, P. C., Heelis, R. A., & Hanson, W. B. (1991). The ionospheric signatures of rapid subauroral ion drifts. *Journal of Geophysical Research*, 96(A4), 5785–5792. <https://doi.org/10.1029/90JA02651>
- Archer, W. E., Gallardo-Lacourt, B., Perry, G. W., St-Maurice, J. P., Buchert, S. C., & Donovan, E. (2019). STEVE: The optical signature of intense subauroral ion drifts. *Geophysical Research Letters*, 46(12), 6279–6286. <https://doi.org/10.1029/2019GL082687>
- Archer, W. E., & Knudsen, D. J. (2018). Distinguishing subauroral ion drifts from birkeland current boundary flows. *Journal of Geophysical Research: Space Physics*, 123(1), 819–826. <https://doi.org/10.1002/2017JA024577>
- Archer, W. E., Knudsen, D. J., Burchill, J. K., Jackel, B., Donovan, E., Connors, M., & Juusola, L. (2017). Birkeland current boundary flows. *Journal of Geophysical Research: Space Physics*, 122(4), 4617–4627. <https://doi.org/10.1002/2016JA023789>
- Bristow, W. A., Hampton, D. L., & Otto, A. (2016). High-spatial-resolution velocity measurements derived using local divergence-free fitting of superdarn observations. *Journal of Geophysical Research: Space Physics*, 121(2), 1349–1361. <https://doi.org/10.1002/2015JA021862>
- Bristow, W. A., Lyons, L. R., Nishimura, Y., Shepherd, S. G., & Donovan, E. F. (2022). High-latitude plasma convection based on superdarn observations and the locally divergence free criterion. *Journal of Geophysical Research: Space Physics*, 127(12), e2022JA030883. <https://doi.org/10.1029/2022JA030883>
- Figueiredo, S., Karlsson, T., & Marklund, G. T. (2004). Investigation of subauroral ion drifts and related field-aligned currents and ionospheric Pedersen conductivity distribution. *Annales Geophysicae*, 22(3), 923–934. <https://doi.org/10.5194/angeo-22-923-2004>
- Foster, J. C., Buonsanto, M. J., Mendillo, M., Nottingham, D., Rich, F. J., & Denig, W. (1994). Coordinated stable auroral red arc observations: Relationship to plasma convection. *Journal of Geophysical Research*, 99(A6), 11429–11439. <https://doi.org/10.1029/93JA03140>
- Foster, J. C., & Burke, W. J. (2002). Saps: A new categorization for sub-auroral electric fields. *Eos, Transactions American Geophysical Union*, 83(36), 393–394. <https://doi.org/10.1029/2002EO000289>
- Gallardo-Lacourt, B., Frey, H. U., & Martinis, C. (2021). Proton aurora and optical emissions in the subauroral region. *Space Science Reviews*, 217(1), 10. <https://doi.org/10.1007/s11214-020-00776-6>
- Gallardo-Lacourt, B., Liang, J., Nishimura, Y., & Donovan, E. (2018a). On the origin of STEVE: Particle precipitation or ionospheric skyglow? *Geophysical Research Letters*, 45(16), 7968–7973. <https://doi.org/10.1029/2018GL078509>
- Gallardo-Lacourt, B., Nishimura, Y., Donovan, E., Gillies, D. M., Perry, G. W., Archer, W. E., et al. (2018b). A statistical analysis of STEVE. *Journal of Geophysical Research: Space Physics*, 123(11), 9893–9905. <https://doi.org/10.1029/2018JA025368>
- Gallardo-Lacourt, B., Perry, G. W., Archer, W. E., & Donovan, E. (2019). How did we miss this? An upper atmospheric discovery named STEVE (No. 100). *Eos*, 100. <https://doi.org/10.1029/2019EO117351>
- Galperin, Y. I. (2002). Polarization jet: Characteristics and a model. *Annales Geophysicae*, 20(3), 391–404. <https://doi.org/10.5194/angeo-20-391-2002>
- Gillies, D. M., Donovan, E., Hampton, D., Liang, J., Connors, M., Nishimura, Y., et al. (2019). First observations from the TREX spectrograph: The optical spectrum of STEVE and the picket fence phenomena. *Geophysical Research Letters*, 46(13), 7207–7213. <https://doi.org/10.1029/2019GL083272>
- Gjerloev, J. W. (2012). The SuperMAG data processing technique. *Journal of Geophysical Research*, 117(A9). <https://doi.org/10.1029/2012JA017683>
- Gonzalez, W. D., Joselyn, J. A., Kamide, Y., Kroehl, H. W., Rostoker, G., Tsurutani, B. T., & Vasyliunas, V. M. (1994). What is a geomagnetic storm? *Journal of Geophysical Research*, 99(A4), 5771–5792. <https://doi.org/10.1029/93JA02867>
- Grocott, A., Cowley, S. W. H., & Sigwarth, J. B. (2003). Ionospheric flow during extended intervals of northward but B y-dominated IMF. *Annales Geophysicae*, 21(2), 509–538. <https://doi.org/10.5194/angeo-21-509-2003>
- Grocott, A., Milan, S. E., Yeoman, T. K., Sato, N., Yukimatu, A. S., & Wild, J. A. (2010). Superposed epoch analysis of the ionospheric convection evolution during substorms: IMF BY dependence. *Journal of Geophysical Research*, 115(A5). <https://doi.org/10.1029/2010JA015728>
- Harding, B. J., Mende, S. B., Triplett, C. C., & Wu, Y.-J. J. (2020). A mechanism for the STEVE continuum emission. *Geophysical Research Letters*, 47(7), e2020GL087102. <https://doi.org/10.1029/2020GL087102>
- He, F., Zhang, X.-X., & Chen, B. (2014). Solar cycle, seasonal, and diurnal variations of subauroral ion drifts: Statistical results. *Journal of Geophysical Research: Space Physics*, 119(6), 5076–5086. <https://doi.org/10.1002/2014JA019807>
- Heelis, R. (2004). Electrodynamics in the low and middle latitude ionosphere: A tutorial. *Journal of Atmospheric and Solar-Terrestrial Physics*, 66(10), 825–838. <https://doi.org/10.1016/j.jastp.2004.01.034>
- Jordanova, V. K., Farrugia, C. J., Fennell, J. F., & Scudder, J. D. (2001). Ground disturbances of the ring, magnetopause, and tail currents on the day the solar wind almost disappeared. *Journal of Geophysical Research*, 106(A11), 25529–25540. <https://doi.org/10.1029/2000JA000251>

- King, J. H., & Papitashvili, N. E. (2005). Solar wind spatial scales in and comparisons of hourly Wind and ACE plasma and magnetic field data. *Journal of Geophysical Research*, 110(A2), A02104. <https://doi.org/10.1029/2004JA010649>
- Knudsen, D. J., Burchill, J. K., Buchert, S. C., Eriksson, A. I., Gill, R., Wahlund, J.-E., et al. (2017). Thermal ion imagers and Langmuir probes in the swarm electric field instruments. *Journal of Geophysical Research: Space Physics*, 122(2), 2655–2673. <https://doi.org/10.1002/2016JA022571>
- Kress, B. T., Rodriguez, J. V., & Onsager, T. G. (2020). Chapter 20 - The goes-r space environment in situ suite (SEISS): Measurement of energetic particles in geospace. In S. J. Goodman, T. J. Schmit, J. Daniels, & R. J. Redmon (Eds.), *The Goes-r Series* (pp. 243–250). Elsevier. <https://doi.org/10.1016/B978-0-12-814327-8.00020-2>
- Laakso, H., & Pfaff, R. (2023). Fast plasma drifts in the high latitude ionosphere. *Geophysical Research Letters*, 50(14), e2023GL103566. <https://doi.org/10.1029/2023GL103566>
- Le, G., Russell, C. T., & Petrinec, S. M. (2000). The magnetosphere on May 11, 1999, the day the solar wind almost disappeared: I. Current systems. *Geophysical Research Letters*, 27(13), 1827–1830. <https://doi.org/10.1029/1999GL010774>
- Ledvina, V., Brandt, L., MacDonald, E., Frisell, N., Anderson, J., Chen, T. Y., et al. (2023). Agile collaboration: Citizen science as a trans-disciplinary approach to heliophysics. *Frontiers in Astronomy and Space Sciences*, 10, 1165254. <https://doi.org/10.3389/fspas.2023.1165254>
- Liang, J., Gillies, D. M., Spanswick, E., & Donovan, E. F. (2024). Converting trex-rgb green-channel data to 557.7 nm auroral intensity: Methodology and initial results. *Earth and Planetary Physics*, 8(1), 258–274. <https://doi.org/10.26464/epp2023063>
- Lin, D., Sorathia, K., Wang, W., Merkin, V., Bao, S., Pham, K., et al. (2021). The role of diffuse electron precipitation in the formation of subauroral polarization streams. *Journal of Geophysical Research: Space Physics*, 126(12), e2021JA029792. <https://doi.org/10.1029/2021JA029792>
- Lynch, K. A., McManus, E., Gutow, J., Burleigh, M., & Zettergren, M. (2022). An ionospheric conductance gradient driver for subauroral picket fence visible signatures near STEVE events. *Journal of Geophysical Research: Space Physics*, 127(12), e2022JA030863. <https://doi.org/10.1029/2022JA030863>
- Lyons, L. R., Nishimura, Y., Liu, J., Yadav, S., Zou, Y., Bristow, W. A., et al. (2024). Space weather with an arc's 2 h trip across the nightside polar cap. *Frontiers in Astronomy and Space Sciences*, 10. <https://doi.org/10.3389/fspas.2023.1309870>
- MacDonald, E. A., Donovan, E., Nishimura, Y., Case, N. A., Gillies, D. M., Gallardo-Lacourt, B., et al. (2018). New science in plain sight: Citizen scientists lead to the discovery of optical structure in the upper atmosphere. *Science Advances*, 4(3), eaq0030. <https://doi.org/10.1126/sciadv.aq0030>
- Martinis, C., Griffin, I., Gallardo-Lacourt, B., Wroten, J., Nishimura, Y., Baumgardner, J., & Knudsen, D. J. (2022). Rainbow of the night: First direct observation of a SAR arc evolving into STEVE. *Geophysical Research Letters*, 49(11), e2022GL098511. <https://doi.org/10.1029/2022GL098511>
- Maynard, N. C., Aggson, T. L., & Heppner, J. P. (1980). Magnetospheric observation of large sub-auroral electric fields. *Geophysical Research Letters*, 7(11), 881–884. <https://doi.org/10.1029/GL007i011p00881>
- Merayo, J. É. M. G., Jørgensen, J. L., Friis-Christensen, E., Brauer, P., Primdahl, F., Jørgensen, P. S., et al. (2008). The swarm magnetometry package. In R. Sandau, H.-P. Röser, & A. Valenzuela (Eds.), *Small Satellites for Earth Observation* (pp. 143–151). Springer Netherlands. https://doi.org/10.1007/978-1-4020-6943-7_13
- Milan, S. E., Hubert, B., & Grocott, A. (2005). Formation and motion of a transpolar arc in response to dayside and nightside reconnection. *Journal of Geophysical Research*, 110(A1). <https://doi.org/10.1029/2004JA010835>
- Mishin, E., & Streltsov, A. (2021). Mesoscale and small-scale structure of the subauroral geospace. In *Ionosphere Dynamics and Applications* (pp. 139–158). American Geophysical Union (AGU). <https://doi.org/10.1002/9781119815617.ch8>
- Mishin, E. V. (2013). Interaction of substorm injections with the subauroral geospace: 1. Multispacecraft observations of said. *Journal of Geophysical Research: Space Physics*, 118(9), 5782–5796. <https://doi.org/10.1002/jgra.50548>
- Mishin, E. V. (2023). The evolving paradigm of the subauroral geospace. *Frontiers in Astronomy and Space Sciences*, 10. <https://doi.org/10.3389/fspas.2023.1118758>
- Mishin, E. V., & Puhl-Quinn, P. A. (2007). Said: Plasmaspheric short circuit of substorm injections. *Geophysical Research Letters*, 34(24). <https://doi.org/10.1029/2007GL031925>
- Nanjo, S., Hofstra, G. A., Shiokawa, K., Shinbori, A., Nozawa, S., & Hosokawa, K. (2024). Post-midnight purple arc and patches appeared on the high latitude part of the auroral oval: Dawnside counterpart of STEVE? *REarth Planets Space*, 76(1), 55. <https://doi.org/10.1186/s40623-024-01995-9>
- Newell, P. T., & Gjerloev, J. W. (2011). Evaluation of supermag auroral electrojet indices as indicators of substorms and auroral power. *Journal of Geophysical Research*, 116(A12). <https://doi.org/10.1029/2011JA016779>
- Newell, P. T., & Gjerloev, J. W. (2014). Local geomagnetic indices and the prediction of auroral power. *Journal of Geophysical Research: Space Physics*, 119(12), 9790–9803. <https://doi.org/10.1002/2014JA020524>
- Nishimura, Y., Dyer, A., Kangas, L., Donovan, E., & Angelopoulos, V. (2023). Unsolved problems in strong thermal emission velocity enhancement (STEVE) and the picket fence. *Frontiers in Astronomy and Space Sciences*, 10. <https://doi.org/10.3389/fspas.2023.1087974>
- Nishimura, Y., Gallardo-Lacourt, B., Zou, Y., Mishin, E., Knudsen, D. J., Donovan, E. F., et al. (2019). Magnetospheric signatures of STEVE: Implications for the magnetospheric energy source and interhemispheric conjugacy. *Geophysical Research Letters*, 46(11), 5637–5644. <https://doi.org/10.1029/2019GL082460>
- Nishimura, Y., Hussein, A., Erickson, P. J., Gallardo-Lacourt, B., & Angelopoulos, V. (2022). Statistical study of magnetospheric conditions for saps and said. *Geophysical Research Letters*, 49(9), e2022GL098469. <https://doi.org/10.1029/2022GL098469>
- Nishimura, Y., Lyons, L. R., Deng, Y., Sheng, C., Bristow, W. A., Donovan, E. F., et al. (2024). Obtaining continental-scale, high-resolution 2-d ionospheric flows and application to meso-scale flow science. *Journal of Geophysical Research: Space Physics*, 129(8), e2024JA032924. <https://doi.org/10.1029/2024JA032924>
- Nishimura, Y., Yang, J., Weygand, J. M., Wang, W., Kosar, B., Donovan, E. F., et al. (2020). Magnetospheric conditions for STEVE and SAID: Particle injection, substorm surge, and field-aligned currents. *Journal of Geophysical Research: Space Physics*, 125(8), e2020JA027782. <https://doi.org/10.1029/2020JA027782>
- Pedatella, N. M., & Larson, K. M. (2010). Routine determination of the plasmopause based on cosmic GPS total electron content observations of the midlatitude trough. *Journal of Geophysical Research*, 115(A9). <https://doi.org/10.1029/2010JA015265>
- Sandholt, P. E., Farrugia, C. J., Moen, J., & Cowley, S. W. H. (1998). Dayside auroral configurations: Responses to southward and northward rotations of the interplanetary magnetic field. *Journal of Geophysical Research*, 103(A9), 20279–20295. <https://doi.org/10.1029/98JA01541>
- Skone, S. H., & Spanswick, E. L. (2023). A multi-scale adaptive data driven ionospheric electron density model for near real-time operations. Retrieved from <https://agu.confex.com/agu/fm23/meetingapp.cgi/Paper/1450123>

- Spanswick, E. L., & Donovan, E. F. (n.d.). Transition region explorer - RGB dataset [Dataset]. University of Calgary. <https://doi.org/10.11575/4P8E-1K65>
- Starr, G., Mrak, S., Nishimura, Y., Hirsch, M., Ishwar, P., & Semeter, J. (2022). Automatic identification of the main ionospheric trough in total electron content images. *Space Weather*, 20(6), e2021SW002994. <https://doi.org/10.1029/2021SW002994>
- Svaldi, V., Matsuo, T., Kilcommons, L., & Gallardo-Lacourt, B. (2023). High-latitude ionospheric electrodynamics during STEVE and non-STEVE substorm events. *Journal of Geophysical Research: Space Physics*, 128(4), e2022JA030277. <https://doi.org/10.1029/2022JA030277>
- Yokoyama, N., & Kamide, Y. (1997). Statistical nature of geomagnetic storms. *Journal of Geophysical Research*, 102(A7), 14215–14222. <https://doi.org/10.1029/97JA00903>
- Zettergren, M. D., & Snively, J. B. (2019). Latitude and longitude dependence of ionospheric TEC and magnetic perturbations from infrasonic-acoustic waves generated by strong seismic events. *Geophysical Research Letters*, 46(3), 1132–1140. <https://doi.org/10.1029/2018GL081569>